

Design and experiment of a bionic vibratory subsoiler for banana fields in southern China

Zhang Xirui¹, Wang Chao¹, Chen Zhishui^{1*}, Zeng Zhiwei²

(1. College of Mechanics and Electrics Engineering, Hainan University, Haikou 570228, China;

2. Department of Biosystems Engineering, University of Manitoba, Winnipeg, Manitoba, Canada, R3T 5V6)

Abstract: Subsoiling is essential in the tillage of banana planting, as banana plants have a fairly sturdy pseudostem and wide row spacing while soil tends to be compacted. In this study, a bionic vibrating subsoiler for banana fields was developed, verified, and evaluated. The vibrator was designed based on crank-rocker mechanism while the bionics design was used for subsoiler development. The forces on the subsoiler were analyzed to verify the strength of the subsoiler tine. To test the performance of the subsoiler, field tests were conducted to measure the draft force and fuel consumption. There was approximately 14% reduction in the draft force and 22% increase in the fuel consumption in vibrating mode compared with that in non-vibrating mode. In conclusion, the study results could be applied in China's tropical agricultural regions.

Keywords: vibratory subsoiler, tillage, simulation, bionics, banana field

DOI: 10.3965/j.ijabe.20160906.1923

Citation: Zhang X R, Wang C, Chen Z H, Zeng Z W. Design and experiment of a bionic vibratory subsoiler for banana fields in southern China. *Int J Agric & Biol Eng*, 2016; 9(6): 75–83.

1 Introduction

Subsoiling, as an important component of vertical tillage, is designed to eliminate the compaction created by horizontal tillage tools such as sweeps and shovel implements. It is a crucial process in conservation tillage which minimizes soil surface disturbance without inversion, while shattering subsoil structure^[1]. Subsoiling breaks up compaction layers, promotes aeration, limits runoff, and increases water holding capacity which helps soil retain moisture. It also alleviates the problem of excessive soil strength by

reducing impedance to root penetration and improving root growth. And subsoiling can significantly enhance soil conservation, water infiltration, and crop yield has been proved^[2-5].

There are mainly two types of subsoilers: non-vibrating (conventional subsoiler), and vibrating (oscillating subsoiler)^[6-8]. Vibrating subsoilers can reduce the draft force, but requires higher overall power than non-vibrating subsoilers since the vibration mechanism demands driving power^[9,10]. In the past decade, studies have been conducted on effects of subsoiling on crop growths and soil properties^[11,12], and the draft reduction of operation^[13,14], as well as modeling and simulation analyses^[15,16]. However, those studies mainly focused on common crops, such as wheat, corn, sugarcane, and cotton, rather than banana plants which are widely cultivated in tropical regions. The existing commercial subsoilers with working width around 1.4-1.8 m cannot work in banana crop fields with plant tall around 2-3.3 m and wide row spacing around 2-2.7 m^[17]. Existing subsoilers were either inefficient in the case of multiple passes with a single subsoiler, or required

Received date: 2015-05-07 **Accepted date:** 2016-10-07

Biographies: **Zhang Xirui**, PhD, Associate Professor, research interests: conservation tillage and tropical agricultural machinery, Email: zhangxirui_999@sina.com; **Wang Chao**, Master student, research interests: tropical agricultural machinery, Email: superwang_999@sina.com; **Zeng Zhiwei**, Master student, research interests: conservation tillage, Email: zengz34@myumanitoba.ca.

***Corresponding author: Chen Zhishui**, Associate Professor, research interests: tropical agricultural machinery, mailing address Hainan University, Haikou, Hainan 570228, China. Email: chenzhishui@hainu.edu.cn.

high-horsepower tractor for pulling a set of subsoilers.

Subsoilers have been evolved to low soil disturbance and low energy input. One of the concepts for design of subsoilers is using the principle of bionics. Soil-burrowing animals, for example, ant (*Formicidae*), house mouse (*Mus musculus*), and pangolin (*M. pentadactyla*), have strong digging legs or claws through natural evolution and adaptation of the living surroundings. Those legs and claws have optimal geometrical features and biomechanical properties, including anti-adhesion, anti-friction, and anti-abrasion properties. Researchers have mimicked the geometrical shapes and curvature characteristics of house mouse's claw in the design of subsoilers to optimize the performance^[18,19].

This research intended to apply the bionic technology and vibrating concept to study the drag reduction performance of the subsoilers, as mentioned above. The research goal was to develop a bionic vibrating subsoiler for banana crop field and study the combined effects of vibrating and bionic of subsoilers, and to promote agricultural mechanization and conservation tillage in China's tropical agricultural regions. The specific objectives of the study were to (1) develop a subsoiler and its vibrating mechanism based on the bionics design concept, (2) perform force analysis on the subsoiler, and (3) evaluate the overall performance of the subsoiler in terms of the draft force and fuel consumption.

2 Material and methods

2.1 Agronomic requirements of subsoiling

The schematic diagram of subsoiling shows the agronomic requirements of the subsoiler designed for banana fields (Figure 1). As banana plants are very tall, subsoiling has to be performed between the plant rows. Banana plants typically have a row spacing of 2500 mm. The subsoiling can be conducted between plant rows with a double-shank subsoiler. The shank spacing was set to 1600 mm, which was considered an appropriate distance away from the banana roots, and at the same time close enough to promote root development and plant growth. The working depth of subsoiler was determined to 350 mm^[20,21] based on the soil layer distribution and

hardpan location in banana fields.

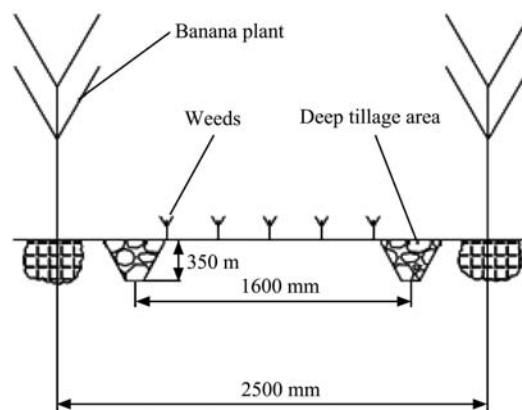


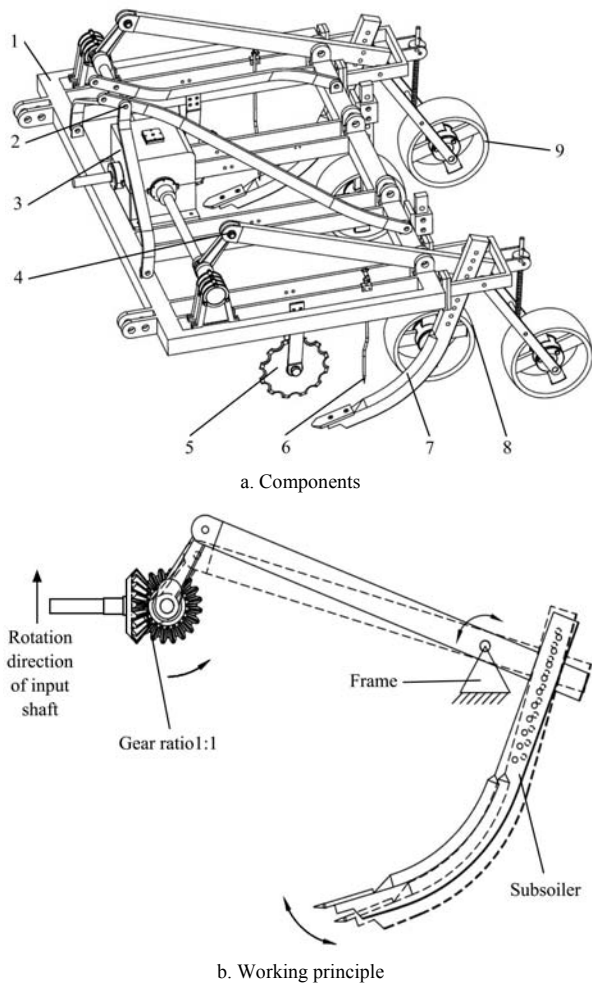
Figure 1 Schematic diagram of subsoiling for banana fields

2.2 Machine description

The subsoilers for wheat, corn, and soybean have been studied quite intensively by using experimental methods and numerical analyses, which provided detailed reference information when designing general components of the subsoiler for banana fields. Therefore, this study only focused on the design and simulation of key components of vibratory subsoiler, i.e. the vibrator and the subsoiler (including the shank and the tine). The feature of double-shank with vibration was adopted to reduce the draft force^[22].

The main components of the subsoiler include frame, gearbox, a pair of suspension brackets, vibrators, coulters, grass breakers, shanks, gauge wheels, and press wheels (Figure 2a). The subsoiler was mounted on the tractor through a three-point hitch. Two vibrators were located symmetrically from the central gearbox at a distance of 1600 mm. Other parameters of the subsoiler are summarized in Table 1.

The vibrators were pivotally coupled with the frame through a pin connection and connected the gearbox and the shank at each end. The working principle of the vibrating subsoiler is illustrated in Figure 2b. Power was transmitted to the input shaft of subsoiler from the tractor PTO (Power Take Off) shaft through a universal joint, and then to the vibrators through the gearbox with a speed reduction ratio of 1. The vibrator was a crank-rocker mechanism, which converted the rotating power of gearbox into reciprocating power of rocker. Thus, the shank attached at the bottom of the rocker gained vibrating motion.



1. Frame 2. Suspension bracket 3. Gearbox 4. Vibrator 5. Coupler
6. Grass breaker 7. Shank 8. Gauge wheel 9. Press wheel

Figure 2 Schematic diagram of subsoiler for banana fields

Table 1 Parameters of the vibratory subsoiler

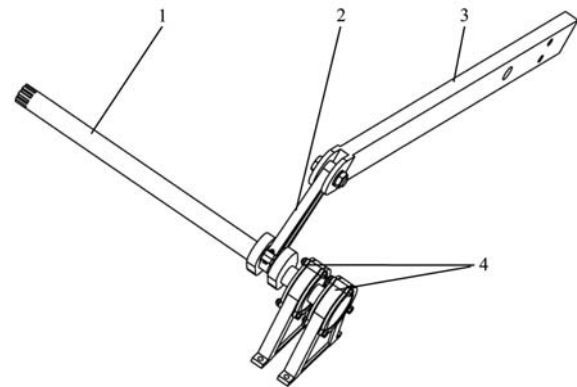
Parameters	Design value
Dimensions (L/W/H)/mm	1950/2000/1230
Weight/kg	250
Power/kW	37-50
Vibrating frequency/Hz	0-9
Working rows	2
Working row space/mm	1600
Working depth/mm	250-350
Working speed/km·h ⁻¹	2.5-6
Efficiency/hm ² ·h ⁻¹	0.375-0.9

2.3 Vibrating system design

The vibrator consists of crankshaft, connecting rod, and rocker, which are shown in Figure 3. The function of the vibrator was to introduce the oscillation in the subsoiler in the longitudinal-vertical plane, i.e. moving forward, backward, upward, and downward.

The crankshaft was connected with output shaft of the gearbox by coupling at one end, and supported by a bearing block at the other end. The crankshaft was made of ductile iron (QT400-10), which had high

strength and toughness with high wear and shock resistance. The crankshaft length (L_0) was determined as 755 mm based on the row spacing (1600 mm) in the banana fields. The eccentricity of crankshaft, i.e. crank length ($L_1 = 40$ mm), was determined empirically to generate practical amplitude of the tine.



Note: 1. Crankshaft 2. Connecting rod 3. Rocker 4. Bearing block

Figure 3 Schematic diagram of the vibrator

A connecting rod was hinged between the crank and the rocker with rod cap and pin connection, respectively. As the main load-bearing component in the crank-rocker mechanism, the connecting rod was made of Q235 steel plate with a thickness of 20 mm. The surface hardness of steel after heat treatment was approximately 302B. The working length of the connecting rod L_2 was chosen as 200 mm. The working distance between the crank and the rocker pivot L_4 was 994 mm, which was determined by the location of fulcrums on the frame.

Rocker was made of Q235 steel plate with hot-rolling and cold-drawing process. The dimensions of the rocker was 1200 mm×80 mm×30 mm (length×width×thickness), while the effective length within the crank-rocker mechanism was L_3 . According to the Grashof's criteria of existing crank in four-bar linkage, the conditions listed below needs to be satisfied:

$$\begin{cases} L_1 + L_4 \leq L_2 + L_3 \\ L_3 \leq L_4 \end{cases} \quad \text{or} \quad \begin{cases} L_1 + L_3 \leq L_2 + L_4 \\ L_4 \leq L_3 \end{cases} \quad (1)$$

Substituting the values and solving the equation set (1) and that L_3 should be greater than 834 mm but less than 1154 mm was obtained. Therefore, the effective length of the rocker was chosen as 885 mm.

2.4 Subsoiler design

2.4.1 Shank design

The subsoiler shank, as the leading soil cutting part,

was developed through quantitatively mimicking the geometrical shapes and curvature characteristics of a house mouse’s digging claw to reduce the draft force of subsoiler. The shank was constituted with a working segment in the middle and two connecting segments at each end, which were used for connecting the rocker and the tine (Figure 4). The #45 steel rod was used to forge the shank. The curve of the working segment was adapted from the amplifying curve of house mouse's claws. The cutting edge of working segment was shaped and sharpened to easily move in the soil. Two connecting segments had rectangular cross-sections and joined with working segments smoothly.

The fitted curve f_1 of the house mouse digging claw was presented as followed^[23]:

$$y = 0.2272 - 5.33522x + 0.62316x^2 - 0.02478x^3 \quad (2)$$

The shank rake angle was obtained between 70.7°-75.6° through the motion analysis of the vibrator. The average value of 73.15° was used. Therefore, the negative tangent value of the shank rake angle was the slope of the tangent line of the working segment upper end, which was close to the rocker.

The working depth and speed of the subsoiler, as well as the soil texture and properties, affected the optimal value of penetrating angle. The common value was within the range of 20°-45° to minimize the working resistance. In consideration of the working conditions in banana fields and the angular fluctuation of 4.9° due to the vibration, the average value of penetrating angle was set to 25°. In other words, the bottom end of the working segment curve had a slope of negative tan 25°.

The equations at two end points, namely points A' and B' , are as follows:

$$\begin{cases} \frac{dy}{dx} = -\tan 25^\circ \\ y = 0.2272 - 5.33522x + 0.62316x^2 - 0.02478x^3 \end{cases} \quad (3)$$

$$\begin{cases} \frac{dy}{dx} = -\tan 73.15^\circ \\ y = 0.2272 - 5.33522x + 0.62316x^2 - 0.02478x^3 \end{cases} \quad (4)$$

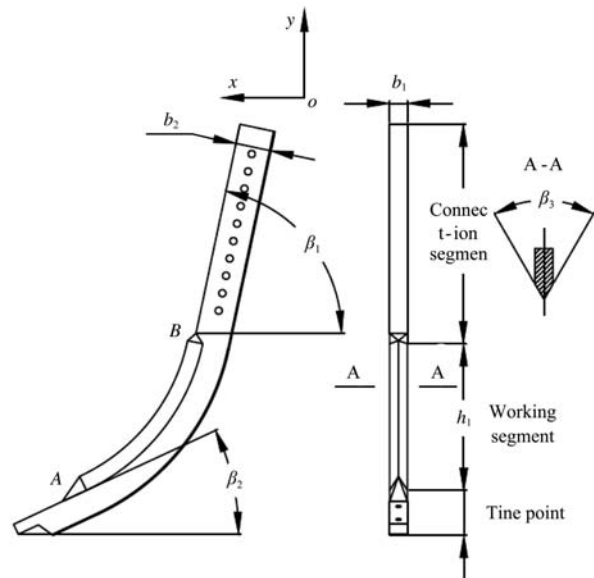
Solving the Equations (3) and (4) and obtained the coordinates of A' (6.19801, -14.80173) and B' (1.83165, -7.60667). The working curve of subsoiler (f_2) was

linearly amplified from the fitted curve of claws (f_1). Assuming the amplification coefficient was n , the corresponding coordinates of A' and B' in f_2 were A (6.19801 n , -14.80173 n) and B (1.83165 n , -7.60667 n), respectively. The maximum subsoiling depth of 350 mm (Table 1) required the vertical height of working segment (h_1) to be 270 mm, in consideration of the height of the bottom connecting segment and the tine. Thus, the height difference between points A and B was 270 mm, i.e. 14.80173 n -7.60667 n =270, which gave an amplification coefficient (n) of 37.52575. The working curve (f_2) for shank was:

$$y = 8.52585 - 5.33522x + 0.01661x^2 - 0.000018x^3 \quad (5)$$

where, 1.83165 n ≤ x ≤ 6.19801 n , i.e. 68.73 ≤ x ≤ 232.58 mm.

The cross-section views of the working segment in Figure 4 showed the cutting angle at the front and the rectangular shape at the back. The cutting angle β_3 of 60° combined with the shank width b_1 of 40 mm and thickness b_2 of 80 mm were used to optimize the subsoiler cutting performance while guaranteeing the tool strength.



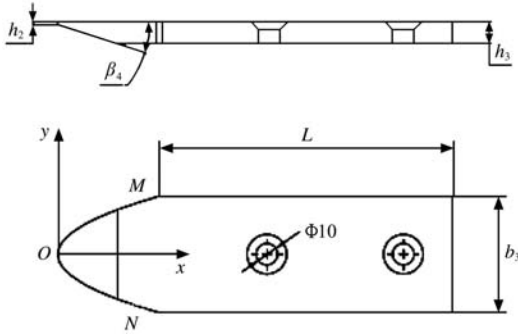
Note: β_1 is the shank rake angle, (°); β_2 is the penetrating angle, (°); β_3 is the cutting angle of the working segment, (°); b_1 is the width of the shank, mm; b_2 is the thickness of the shank, mm; h_1 is the length of working segment in the vertical direction, mm.

Figure 4 Schematic diagram of the subsoiler shank

2.4.2 Tine design

To minimize the soil resistance and have better wear resistance, the subsoiler tine was developed based on the shape of soil-burrowing animal toes. A blade-like

structure with a strong burrowing ability was chosen, while a parabolic curve was used for front and a rectangular shape was used for the back (Figure 5). Considering the heavy residue in banana fields, two countersunk screws were placed in the countersink holes to fasten the tine at the tip of shank. The flat surface of the tine improved soil and residue flows and prevented tool from clogging. The tine was made of 65Mn steel with post-quenching.



Note: β_4 is the cutting angle of the tine, ($^\circ$); h_2 is the thickness of the tine tip, mm; h_3 is the thickness of the tine base, mm; L is the length of the tine base, mm; b_3 is the width of the tine, mm.

Figure 5 Schematic diagram of the subsoiler tine

The parabolic tip can be described using the following equation from the coordinates shown in Figure 5.

$$y^2 = 0.2887b_3x, \left(-\frac{b_3}{2} \leq y \leq \frac{b_3}{2}\right) \quad (6)$$

The draft force and subsoiling width were both positively related to the width of the tine. To achieve desired working width under acceptable soil resistance, the width of the tine b_3 was set to 60 mm. The length of the tine base L was set to 150 mm to ensure the reliability of the connection between the shank and the tine.

Decreasing the thickness of the tine tip would reduce soil resistance during cutting operations. However, a curved shape was relatively easy to create using a thin tip. The thickness h_2 was set to 2 mm for the tine tip. The thickness of the tine base h_3 was chosen to 12 mm in consideration of strength as well as light weight.

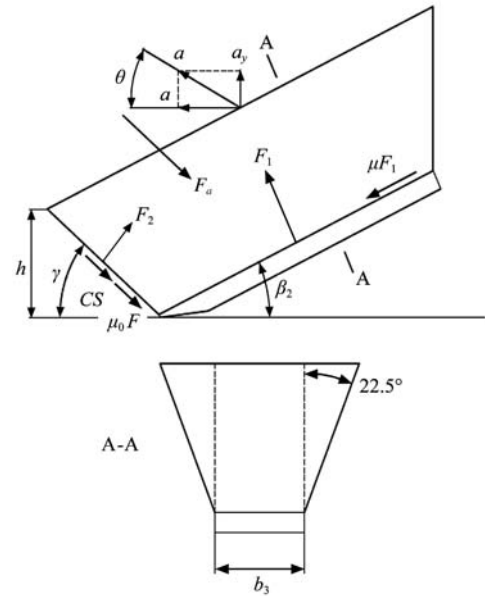
The cutting angle of the tine affected the cutting resistance in soil, while decreasing the cutting angle reduced the overall strength. The cutting angle of the tine was usually less than the penetrating angle to prevent compaction during subsoiling operations. Considering the fluctuation of penetrating angle, the cutting angle of the tine β_4 was determined to be 18° .

2.5 Force analysis

2.5.1 Subsoiler force analysis

The shank and the tine are the major load carrying components of the subsoiler, and the tine encounters a more complicated and unfavorable stress situation in the sub-soil surface. Thus, the force analysis was conducted on the tine via simulation to validate its working state in terms of material strength properties.

Under the action of vibrating and cutting tine, the forces acting upon the clod located above the tine includes gravity, accelerating force, shear force, and the normal and frictional force due to the interaction with the tine and the front soil clod (Figure 6). The soil was assumed to be homogeneous and free of stones which had a negligible shear force. The fluctuation of 4.9° in penetrating angle would not affect the force analysis. Thus the average penetrating angle of 25° was used for simplicity.



Note: F_1 is the normal force from the tine, N; F_2 is the normal force from the front soil clod, N; F_a is the accelerating force, N; β_2 is the penetrating angle, ($^\circ$); γ is the rake angle of the failure plane, ($^\circ$); μ is the friction coefficient between soil and the tine; μ_0 is the friction coefficient of soil; C is the soil cohesion, N·m⁻²; S is the area of the failure plane, m²; a is the acceleration of the clod, m·s⁻²; a_x is the acceleration of the clod in horizontal direction, m·s⁻²; a_y is the acceleration of the clod in vertical direction, m·s⁻².

Figure 6 Force analysis of the clod above the tine

The mechanics equilibrium equations in the horizontal and vertical directions of the clod are based on Newton's second law:

$$\begin{aligned} F_1 \cos \beta_2 + F_1 \mu \sin \beta_2 + F_2 \cos \gamma \\ - (F_a + CS + \mu_0 F_2) \sin \gamma - \rho V g = \rho V a_x \end{aligned} \quad (7)$$

$$F_1 \sin \beta_2 + F_1 \mu \cos \beta_2 - F_2 \sin \gamma - (F_a + CS + \mu_0 F_2) \cos \gamma = \rho V a_y \quad (8)$$

where, ρ is the soil density, kg/m^3 .

The acceleration of the clod under the impact of the tine can be expressed by the following equations:

$$a_y = a \sin \theta \quad (9)$$

$$a_x = a \cos \theta \quad (10)$$

$$a = a' \quad (11)$$

where, a' and a are the acceleration of the tine and the clod respectively, m/s^2 .

The accelerating force of the clod based on the Newton's second law is:

$$F_a = m_1 \frac{dv}{dt} \quad (12)$$

where, m_1 is the mass of the clod, kg .

The movement of the clod was simplified as a uniformly accelerated motion:

$$\frac{dv}{dt} = \frac{v_2}{t} \quad (13)$$

$$v_0 - v_1 \cos \beta_2 - v_2 \cos \gamma = 0 \quad (14)$$

$$v_2 \sin \gamma - v_1 \sin \beta_2 = 0 \quad (15)$$

The speed increased from zero to v_2 within the accelerating time (t). The vertical amplitude of the tine was negligible in comparison with the subsoiling depth. Therefore, the mass of the clod under acceleration was approximated as the mass of the soil disturbed by the subsoiler, which was calculated as:

$$m_1 = \rho b_3 h v_0 t \quad (16)$$

where, v_0 is the working speed of the subsoiler, $v_0 = 2.5\text{-}6.0 \text{ km/h}$ ($0.7\text{-}1.7 \text{ m/s}$).

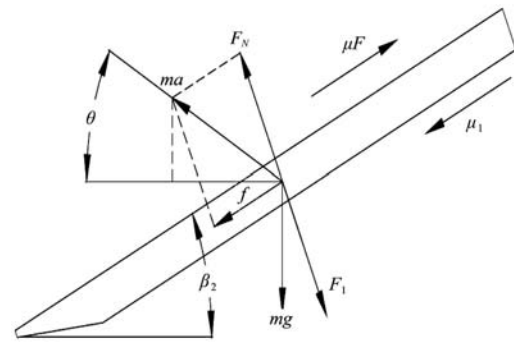
Solving the Equations (12) to (16) simultaneously and get the expression of the accelerating force as:

$$F_a = \frac{\rho b_3 h v_0^2}{\sin \gamma \left(\frac{1}{\tan \beta_2} + \frac{1}{\tan \gamma} \right)} \quad (17)$$

The force acting on the tine could be partitioned into gravity, and the normal and frictional force from the interaction between the clod and the shank (Figure 7). The mechanics equilibrium equations in horizontal and vertical directions of the tine are:

$$f = \mu_1 F_N - \mu F_1 \quad (18)$$

$$f + mg \sin \beta_2 = ma' \sin(\theta + \beta_2) \quad (19)$$



Note: F_N is the normal force from the shank, N ; F_1 is the normal force from the clod above, N ; f is the resultant friction force, N ; β_2 is the penetrating angle, ($^\circ$); θ is the angle between the tine acceleration and the horizontal plane, ($^\circ$); μ is the friction coefficient between the clod and the tine; μ_1 is the friction coefficient between the tine and the shank; m is the mass of the tine, kg .

Figure 7 Force analysis of the tine

2.6 Field tests

Field performance tests of the subsoiler prototype were conducted in the banana fields, which locate in the Baodao Village, Danzhou City, Hainan Province, China. The plant spacing and row spacing was 1400 mm and 2500 mm, respectively. The average diameter of the pseudostems and the height of the plants were 375 mm and 2500 mm, respectively. The soil was sandy clay loam (58% sand, 20% silt, and 22% clay). The average moisture content of the soil within the depth range from 0 to 400 mm was 30.3%.

A subsoiler-tractor-dynamometer-tractor structure was used to measure the draft force of the subsoiler prototype in the tests. The subsoiler was mounted on a towed tractor (Shanghai 504 tractor). A second tractor (Dongfanghong 554 tractor) was used to pull the first tractor through a HP-50k digital dynamometer to measure the draft force. The rolling resistance of the towed tractor was measured without hauling the subsoiler. Then, the draft force of subsoiler was obtained by subtracting the rolling resistance. Both vibrating and non-vibrating modes were tested at three working depths of 200 mm, 300 mm, and 400 mm, respectively. Each treatment was replicated five times. The plot width was one pass of the subsoiler and the plot length was 80 m. For each pass, the middle 40 m section was used for draft force measurements. This left a 20 m buffer area at each end for tractor acceleration and deceleration. Within the middle section of the plot, the tractor travelled at a constant speed of 1 m/s. An ultrasonic sensor HTYH01 was used as transducer to detect the oil-level, by which

the fuel consumption was determined.

3 Results and discussion

3.1 Subsoiler force analysis

The mass of the clod was a product of the soil density and the volume of the soil being supported by the tine, which was the volume of a frustum-like geometry (Figure 7). The area of the failure plane ($S=129000-225000 \text{ mm}^2$) and the volume of the clod ($V=23420000-49840000 \text{ mm}^3$) within the range of subsoiling depth ($h=250-350 \text{ mm}$) were obtained through three dimensional (3 D) modeling. The soil density ($\rho=1150 \text{ kg/m}^3$) and cohesion ($C = 20000-40000 \text{ N/m}^2$) in the banana field were measured using standard methods. The friction coefficient between the tine and the shank ($\mu_1=0.15$), the distance between the tine and the rocker pivot ($r=745 \text{ mm}$), and the mass of the tine ($m=0.897 \text{ kg}$) were also measured. The friction coefficient between the tool and the soil: $\mu=0.4-0.6$ ^[24], and that of the soil: $\mu_0=0.56$ ^[25], as well as the rake angle of the failure plane: $\gamma=52^\circ$ ^[26] were obtained from the literature. The angle between the tine acceleration and the horizontal plane was calculated as $\theta=\theta_3-90^\circ-\beta_1+\beta_2=27.24^\circ$ when the tine acceleration (a) and the rocker angular acceleration (α_3) had maximum values of: $a_{\max}=130.2564 \text{ m/s}^2$ and $\alpha_{3\max}=174.8408 \text{ rad/s}^2$.

Substituting those values into the Equations (9) to (11) and (17) to (19) and simultaneously solving for the applied forces experienced by the tine, the maximum value of the normal forces and friction forces on both top and bottom sides of the tine were $F_{1\max}=6525 \text{ N}$, $F_{N\max}=26716 \text{ N}$, $\mu F_1 = 3915 \text{ N}$, and $\mu_1 F_N = 4007 \text{ N}$.

3.2 Field test results

The draft force was sampled per second during

operation and plotted in Figure 8. The vibrating subsoiler had relatively smaller draft force at almost all the sampling points, which implied that the vibration reduced the draft force. However, the fuel consumption per unit area in Table 2 showed that the vibrating mode consumed more fuel than the non-vibrating mode. The reduction coefficient of draft force (η_r) and the increase coefficient of fuel consumption (η_o) were calculated as follows:

$$\eta_r = \frac{\bar{P}_e - \bar{P}_v}{\bar{P}_e} \times 100\% \tag{20}$$

$$\eta_o = \frac{Q_v - Q_e}{Q_e} \times 100\% \tag{21}$$

where, the subscripts v and e represent vibrating and non-vibrating modes, respectively.

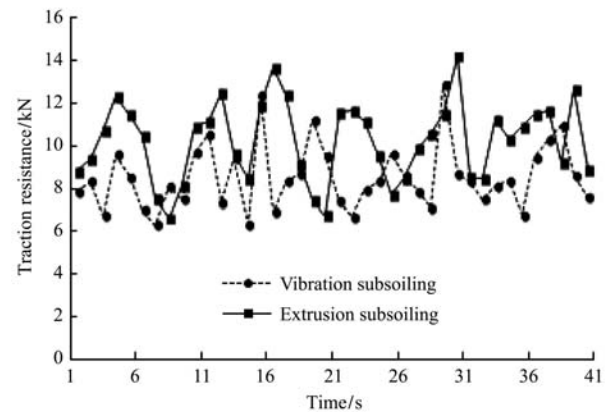


Figure 8 Draft force under vibrating and non-vibrating modes at subsoiling depth of 400 mm

The results in Table 2 showed that under the vibrating mode, the draft force was reduced ranging from 10% to 17%, whereas it increased the fuel consumption ranging from 16% to 27% depending on the working depths. These findings occurred under the working speed of 1 m/s and PTO of 540 r/min.

Table 2 Comparisons of draft force and fuel consumption at different subsoiling depths

Subsoiling depth/mm	Draft force			Fuel consumption		
	Average in vibrating mode/kN	Average in non-vibrating mode/kN	Decrease /%	Average in vibrating mode/(L·hm ⁻²)	Average in non-vibrating mode/(L·hm ⁻²)	Increase /%
200	3.5365	4.0540	12.77	11.46	9.52	20.38
300	6.2153	6.9535	10.61	21.25	16.78	26.64
400	8.5435	10.2272	16.46	28.21	24.12	16.96

4 Conclusions

The bionic vibrating subsoiler was developed based on the agronomic requirements of banana planting. The

structure was simple, yet reliable, and the tractor provided vibrating power for the subsoiler through the PTO shaft. The draft force required for subsoiling was reduced through bionics design of the shank and the tine. The

field tests under the vibrating and the non-vibrating modes showed that the average draft force decreased by approximately 13% and the average fuel consumption increased by 21%, at the different depths, in case of vibration at a tractor speed of 1 m/s and PTO 540 r/min. The results are comparable to the 13%-18% draft force reduction of 1SZ-460 lever-type subsoiler^[27] and 8.5%-39.5% draft force reduction of a bionic anti-drag subsoiler^[28], which the combined effects of banana crop subsoiling similar to the separate application results of the bionic technology or vibrating concept for major crops (maize, wheat, rice, et al.) may be due to the shallow rooted characteristics and a wide distribution root systems of banana crop that caused a greater resistance need further research. Besides, the vibrating design reduced the draft force, whereas it required higher fuel consumption, which was similar to the findings of Zhang et al.^[29] The method and power used to drive the vibrator needs further research to balance the draft and energy requirements, and improve the overall efficiency. As the vibrating frequency and amplitude affected the magnitude of the draft, further understanding their relationship is also recommended.

Acknowledgments

This work was financed by the Special Fund for Agro-scientific Research in the Public Interest from the Ministry of Agriculture, China (Grant No.201503136), the National Natural Science Foundation of China (Grant No.51565010) and the National Natural Science Foundation of Hainan Province (Grant No.20163038). Thanks are given to Dr. Ying Chen from the Department of Biosystems Engineering, University of Manitoba, Canada for her assistance in the experiment.

[References]

- [1] Ehlers W, Claupein W. Approaches towards conservation tillage in Germany. In: Carter M R (Ed.), *Conservation Tillage in Temperate Agroecosystems*. Lewis Publishers, Boca Raton, USA, 1994; pp. 141–165.
- [2] Abo-Elnor M, Hamilton R, Boyle J T. Simulation of soil-blade interaction for sandy soil using advanced 3D finite element analysis. *Soil and Tillage Research*, 2004; 75(1): 61–73.
- [3] Evans S D, Lindstrom M J, Voorhees W B, Moncrief J F, Nelson G A. Effect of subsoiling and subsequent tillage on soil bulk density, soil moisture, and corn yield. *Soil Till*, 1996; 38(1-2): 35–46.
- [4] Mouazen A M, Ramon H. A numerical-statistical hybrid modelling scheme for evaluation of draught requirements of a subsoiler cutting a sandy loam soil, as affected by moisture content, bulk density and depth. *Soil & Tillage Research*, 2002; 63(3-4): 155–165.
- [5] Harisson H P, Licsko Z J. Soil reacting wrenches and dynamics for three models of bent leg plows. *Transactions of the ASAE*, 1989; 32(1): 50–53.
- [6] Sakai K, Hata S I. Design parameters of four-shank vibrating subsoiler. *Transactions of the ASAE*, 1993; 36(1): 330–336.
- [7] Wang G, Jia H L, Tang L, Zhuang J, Jiang X M, Guo M Z. Design of variable screw pitch rib snapping roller and residue cutter for corn harvesters. *Int J Agric & Biol Eng*, 2016; 9(1): 27–34.
- [8] Tong J, Moayad B Z. Effects of rake angle of chisel plough on soil cutting factors and power requirements: A computer simulation. *Soil & Tillage Research*, 2006; 88(1-2): 55–64.
- [9] Linde J V D. Discrete element modeling of a vibratory subsoiler. Stellenbosch University of Stellenbosch, 2007.
- [10] Shchukin S G, Nagajka M A. Investigation of the soil tillage process by vibratory subsoiler. *Siberian Herald of Agricultural Science*, 2015: 83–89.
- [11] He J, Li H W, Mao N, Wang S D. Experimental study on combined operation of drilling and subsoiling for no-till maize. In: *The 2004 CIGR International Conference*, Beijing, China, October, 2004; pp. 188–193.
- [12] Tjink F J, Van J P. Engineering approaches to prevent subsoil compaction in cropping systems with sugar beet. In: Horn R, vanden Akker J J H, Arvidsson J (Eds.), *Subsoil Compaction. Advances in Geocology*, vol.32. Catena Verlag, Reiskirchen, 2000; pp. 442–452.
- [13] Li X, Fu J F, Zhang D X. Experiment analysis on traction resistance of vibration subsoiler. *Transactions of the CSAE*, 2012; 28(1): 32–36. (in Chinese with English abstract)
- [14] Li B, Xia R, Liu F Y, Chen J, Han W T, Han B. Determination of the draft force for different subsoiler points using discrete element method. *Int J Agric & Biol Eng*, 2016; 9(3): 81–87
- [15] Mouazen A M, Nemenyi M. Finite element analysis of subsoiler cutting in non-homogeneous sandy loam soil. *Soil & Tillage Research*, 1999; 51(1-2): 1–15.
- [16] Shmulevich I, Asaf Z, Rubinstein D. Interaction between soil and a wide cutting blade using the discrete element method. *Soil & Tillage Research*, 2007; 97(1): 37–50.
- [17] Huang K L. High quality and high yield cultivation

- techniques of banana. Guangdong Agricultural Sciences, 2010; 37(10): 69–70. (in Chinese with English abstract)
- [18] Tong J, Chen D H, Tomoharu Y, Zhang S J, Ren L Q. Geometrical features of claws of house mouse *Mus Musculus* and biomimetic design method of subsoiler structure. Journal of Bionic Engineering, 2005; 8(1): 53–63.
- [19] Zhang J B, Tong J, Ma Y H. Simulation of bionic anti-drag subsoiler with exponential curve feature using discrete element method. Applied Mechanics and Materials, 2013; 461: 535–543.
- [20] Linde J V D. Discrete element modeling of a vibratory subsoiler. Stellenbosch University of Stellenbosch, 2007: 49–53.
- [21] Shahgoli G, Fielke J, Saunders C, Desbiolles J. Simulation of the dynamic behaviour of a tractor-oscillating subsoiler system. Biosystems Engineering, 2010; 106(2): 147–155.
- [22] Li L X, Ji H L. Nonlinear dynamics analysis of vibratory subsoiler. Information Technology Journal, 2013; 12(15): 3224–3228.
- [23] Chen D H. Typical bio-tribological structures and their biomimetic applications. Changchun: Jilin University, 2007.
- [24] Gong H Y, Wang L Q, Xing X D. Modeling of the plow body of submarine plowing trencher and analysis of the soil cutting process. Journal of Mechanical Engineering, 2012; 48(19): 134–139. (in Chinese with English abstract)
- [25] Zhou Y Q. Force Mathematical Model and Computer Simulation of the subsoiler. Zhengzhou: Henan Agricultural University, 2006.
- [26] Mak J, Chen Y, Sadek M A. Determining parameters of a discrete element model for soil–tool interaction. Soil and Tillage Research, 2012; 118(5): 117–122.
- [27] Li Y L, Liu B, Cui T, Zhang D X. Design and field experiment on 1SZ- 460 lever type subsoiler. Transactions of the CSAM, 2009; 40(S1): 37–40. (in Chinese with English abstract)
- [28] Zhang J B, Tong J, Ma Y H. Design and experiment of bionic anti-drag subsoiler. Transactions of the CSAM, 2014; 45(4): 141–145. (in Chinese with English abstract)
- [29] Zhang Z J, Jia H L, Sun J Y. Review on application of biomimetic for designing soil-engaging tillage implements in Northeast China. Int J Agric & Biol Eng, 2016; 9(4): 12–21.